Unique Word OFDM with Joint Time-Frequency Channel Estimation for Internet of Underwater Things

Zeyad A. H. Qasem, Xingbin Tu, Chunyi Song, Fengzhong Qu, Waheb A. Jabbar and Hamada Esmaiel

***Abstract*- The acoustic-based internet of underwater things (IoUT) is considered as one of the most challenging environments for communication because of issues in the underwater acoustic communication (UWAC) channel, such as multipath propagation and Doppler shift. Accurately estimating these effects without sacrificing a significant portion of the bandwidth is extremely difficult, underscoring the need for robust and sophisticated techniques. In this paper, we propose an acoustic-based unique word orthogonal frequency division multiplexing (UW-OFDM) scheme to enable communication between IoUT nodes over a doubly-selective channel. The proposed scheme employs a joint time-frequency channel estimation approach by leveraging the time-domain guard interval to identify the channel paths while utilizing only 3.1% of the frequency-domain subcarriers, compared to 25% in conventional methods, to track the channel path coefficients. The proposed method significantly enhances spectral efficiency while maintaining resilience to multipath propagation and Doppler shift impairments inherent in UWAC. Furthermore, the scheme eliminates inter-block interference, which is critical in UWAC due to its distinctive propagation characteristics. We evaluate the performance of the proposed methods using both simulations and real-world experimental tests over a 300-meter underwater channel. The results demonstrate that the proposed approach offers a reliable IoUT communication solution, achieving up to a 5 dB improvement in bit error rate and up to 17.56% higher subcarrier utilization compared to conventional schemes. In addition, the scheme exhibits strong robustness against Doppler shift effects with similar peak-to-average power ratio performance and a modest increase in computational complexity.**

***Index Terms*— Underwater communication, channel estimation, IoUT, time-frequency processing, and bandwidth efficiency.**

I. Introduction

RECENT advancements in underwater acoustic communication (UWAC) have sparked the emergence of the internet of underwater things (IoUT), a transformative paradigm that extends IoT frameworks into aquatic environments [1, 2]. The emergence of IoUT has led to the increased utility of advanced UWAC systems for various tasks, including seabed mapping, monitoring ocean currents, and military surveillance. Fig. 1 shows how these uses depend on networks of IoUT-enabled devices, such as autonomous underwater vehicles (AUVs), underwater gliders, and smart sensor nodes, that work together to collect and transmit data over vast ocean areas. However, the efficacy of IoUT ecosystems relies on overcoming persistent UWAC challenges, such as severe multipath interference and Doppler shift (DS). These distortions arise from the difficulty in controlling the movement of IoUT devices and the inherent properties of underwater sound propagation, including its low velocity (~1500 m/s) and reflections from the water surface, which dramatically degrade communication reliability. To ensure robust control and coordination of IoUT devices, advanced channel tracking techniques are imperative to mitigate these effects and maintain reliable connectivity. By addressing these barriers, IoUT stand to revolutionize underwater monitoring, bridging the gap between terrestrial IoT and marine environments while unlocking unprecedented opportunities for sustainable ocean exploration and resource management [3, 4].

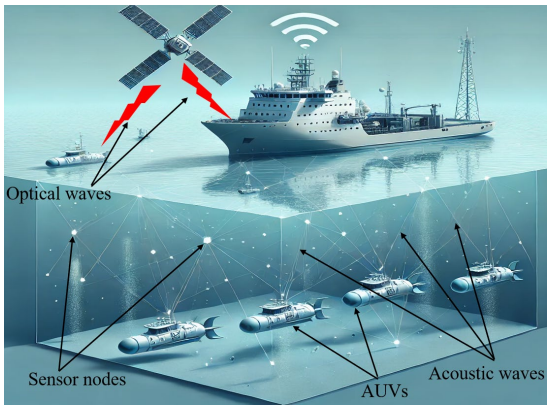

Fig. 1: Illustration of an IoUT System.

Orthogonal frequency division multiplexing (OFDM) is presented as an attractive choice for UWAC due to its significant robustness to multipath interference, low-complexity channel equalization, and high spectral efficiency [5, 6]. However, the performance of OFDM in an UWAC environment is significantly degraded by changing channel conditions that create uneven distribution and loss of orthogonality between the OFDM subcarriers [7-9]. Multipath propagation and Doppler shift are among the most challenging issues to address in UWAC communication. The nature of underwater channels is unpredictable and characterized by long-delay, sparse components [10]. In contrast to short-distance UWAC, long-distance UWAC features a broader variety of channel impulse responses (CIRs), ranging from simple to complex configurations. The CIRs associated with short-range UWAC are usually sparse [5]. However, UWAC

(Corresponding author: Fengzhong Qu*)*

Zeyad A. H. Qasem, Xingbin Tu, Chunyi Song and Fengzhong Qu are with Donghai Laboratory, Zhoushan 316000, China, and also with the Ocean College, Zhejiang University, Zhoushan 316021, China (e-mail: zeyadqasem@zju.edu.cn; xbtu@zju.edu.cn, cysong@zju.edu.cn, and jimqufz@zju.edu.cn).

Waheb A. Jabbar is with College of Engineering, Faculty of Computing, Engineering and the Built Environment, Birmingham City University, Birmingham B4 7XG, West Midlands, England, United Kingdom. (email: waheb.abdullah@bcu.ac.uk).

Hamada Esmaiel is with Electrical Engineering Department, College of Engineering, King Khalid University, Abha 61411, Saudi Arabia; and with the Electrical Engineering Department, Faculty of Engineering, Aswan University, Aswan 81542, Egypt. (Emails: h.esmaiel@aswu.edu.eg).

applications based on IoUT are expected to operate over varying distances, making it particularly difficult to classify the maximal delay and effective paths of the channel. As a result, adopting the corresponding channel estimator to accurately track the UWAC channel without significant overhead becomes highly complicated.

Generally, the UWAC channel effects are tracked by recovering the DS and multipath effects. In terms of DS estimation and compensation, the process includes compensating the coarse DS by a resampling operation followed by estimating the remaining residual DS [11], i.e., the carrier frequency offset (CFO) [12], using pilot subcarriers and/or null subcarriers [8, 13]. This estimation method is essential for maintaining the integrity of the transmitted signal, as any residual DS can significantly impair system performance. Thus, precise CFO prediction is crucial for maintaining dependable communication, especially in settings with fluctuating channel conditions. The approach based on pilot subcarriers [8] utilizes a non-linear least square (NLS) to estimate the residual DS and CIRs. Although this approach avoids the reduction of bandwidth efficiency, it comes at the cost of high computational complexity and poorer performance in harsh UWAC channels [7, 14]. The other approach in [12] suggests using null symbols in the frequency domain to track the CFO effect, while pilot symbols are used to track the CIRs. Consequently, a reliable CFO estimation can be guaranteed in practical UWAC systems, albeit at the expense of a lower data rate. On the other hand, multipath estimation plays an essential role in achieving a reliable UWAC system. For example, when considering the UWAC channel to be sparse, its diversity can readily be exploited by means of compressive sensing (CS), i.e., orthogonal matching pursuit (OMP) [15, 16], simultaneous orthogonal matching pursuit (SOMP) [16, 17], and subspace pursuit [18, 19]. Alternatively, the least squares [20] and adaptive algorithms [21, 22] can tune the coefficients of non-sparse CIRs to find the optimal solution. Although CS can track the sparse UWAC well, it requires a longer pilot than the channel delay. In practical scenarios, the unpredictable channel delay necessitates a longer pilot. Unfortunately, this results in a loss in the already limited efficiency of UWAC bandwidth, necessitating the search for other multi-carrier methods that can handle the residual effects of the channel.

Several schemes have been adopted for UWAC to avoid the sensitivity to channel effects while ensuring efficient subcarrier utilization [5, 6, 14-16]. In [5], we utilized a real OFDM signal that employs the Hartley transform instead of fast Fourier transform (FFT) to improve the robustness of OFDM to the residual DS effect, albeit at the expense of higher peak-to-average power ratio (PAPR) performance. Precoded OFDM has also been investigated in UWAC to overcome the PAPR issue and harvest the maximum diversity of multipath UWAC channel [6, 14] at the expense of greater sensitivity to the residual channel effect. The impact of precoded OFDM is justified by the distribution of errors among all subcarriers due to the use of the unitary precoder with modulated data. Time-domain CS has been used for UWAC along with time-domain synchronous OFDM (TDS-OFDM) in [6, 16] to improve subcarrier utilization by avoiding the use of frequency-domain pilots. However, these schemes assume the channel delay and sparsity level are precisely known, and they require that a portion of the time-domain guard interval be completely free from inter-block interference (IBI), which is often impractical. Furthermore, directly inserting known sequences into UWAC systems to serve as guard intervals and for channel estimation introduces a significant challenge of IBI between these inserted sequences and the adjacent data blocks [6, 15]. Moreover, the time-domain channel estimation (CE) provided by TDS-OFDM becomes inferior to frequency-domain CE in harsh environments, as we will demonstrate shortly later. Joint time-frequency CE for TDS-OFDM is presented in [23, 24]. However, the effect of IBI, which is difficult to remove in UWAC systems, significantly limits the performance of this scheme. The degradation makes the TDS-OFDM schemes less attractive for use in UWAC systems.

Recently, unique word OFDM (UW-OFDM) has been introduced to offer many advantages such as (i) inheriting lower out-of-band radiation and providing diversity gain compared to cyclic prefix OFDM (CP-OFDM) [25-28]; (ii) overcoming the critical issue present in TDS-OFDM by inserting the time-domain guard interval in frequency domain to be a predetermined sequence within the time-domain discrete Fourier transform (DFT) interval; and (iii) providing better bit error rate (BER) performance due to the diversity gain introduced in the UW-OFDM data structure [29]. Despite the development of various strategies to enhance the performance of UW-OFDM, challenges persist, particularly with the high PAPR effect. Additionally, a thorough investigation of these strategies with time and/or frequency domain CE in practical UWAC systems is still lacking. In [28], we enabled the integration of UW-OFDM into UWAC through the implementation of the X-transform and a one-step guard interval insertion. However, the time-domain CE used in this approach shares the same limitations as those identified in TDS-OFDM. To the best of the authors' knowledge, no thorough study has been conducted on how UW-OFDM can help with the changing conditions of UWAC channels.

In this paper, we first introduce a new UWAC scheme based on UW-OFDM, called time-domain UW-OFDM (TD-UW-OFDM), which involves CS-based CE using the time-domain guard interval. This scheme utilizes the IBI-free portion to estimate the UWAC channel, eliminating the need for additional overhead. However, in harsh UWAC, the channel delay might be almost the same as the time-domain guard interval with a strong residual DS effect, which leads to performance degradation of the TD-UW-OFDM. To solve this problem, we introduce a new method called time-frequency-based channel estimation for UW-OFDM (TFCE-UW-OFDM), where we add very short frequency-domain pilots without the need for extra processing, creating a specific sequence that fits within the time-domain guard interval. Then, frequency-domain pilots and time-domain guard interval are jointly used to identify the delay and the optimal path coefficients of the UWAC channel, respectively. Consequently, effective tracking of the UWAC channel with optimal overhead is enabled. The contributions of our paper can be summarized as follows:

- We introduce the TD-UW-OFDM scheme for doubly selective IoUT system. Channel estimation and

equalization are enabled using only the time-domain guard interval, leading to enhancements in the UWAC system in terms of spectral efficiency and robustness to the channel variations.

- A novel time-frequency channel estimation that jointly tracks the UWAC channel effects in IoUT systems has been proposed. Inspired by the sparse UWAC channel and the time-domain processing in the first part of our contribution, this approach jointly leverages both frequency and time-domain processing for efficient tracking of channel effects. For instance, the time-domain guard interval is employed for estimating the channel paths while only 3.1% of the available frequency-domain subcarriers are utilized to track the channel path coefficients instead of 25% in the conventional OFDM-based UWAC systems. Consequently, we can achieve a reliable UWAC system through this joint time-frequency processing without consuming a significant portion of the available bandwidth for overhead.
- Extensive simulation and experimental tests have been conducted in the sea over a distance of 300 meters (m) to validate the feasibility of the proposed approaches.

The structure of this paper is outlined as follows: Section II presents the UWAC system-based TD-UW-OFDM. Section III details the TFCE-UW-OFDM system model. Section IV analyzes the performance of the proposed schemes. Section V provides both simulation and real experimental results. Finally, the conclusion is drawn in Section VI.

II. UWAC-BASED TD-UW-OFDM SYSTEM MODEL

Let's consider each UW-OFDM symbol contains a number of subcarriers $N = N_d + N_r + N_z$, in which N_r are the redundant frequency-domain subcarriers used to produce well-defined sequences in the time domain with length N_u and $N_r \geq N_u$, N_d are the subcarriers that carry modulated information data $\mathbf{d} \in \mathbb{C}^{N_d \times 1}$, and N_z are zero subcarriers that can be used to track the CFO effect and/or enable frequency-domain oversampling. As shown in Fig. 2, the guard interval in UW-OFDM embedded within the DFT interval, unlike the traditional guard intervals in CP-OFDM and TDS-OFDM. In conventional OFDM, a separate guard interval must be added in time domain after the DFT procedure. Despite the use of a well-known time-domain guard interval, UW-OFDM also enables circular convolution with the channel without any IBI effects. However, the received symbol structure will also be different as shown in Fig. 3. For example, the well-known time-domain sequences in UW-OFDM will experience such IBI due to the UWAC channel delay. The IBI effect seen in TDS-OFDM and TFT-OFDM [16, 23], causes severe performance degradation since it cannot be subtracted in harsh UWAC environments. Thus, the time-domain UW-OFDM signal, that represents the output of IFFT, $\mathbf{s}' \in \mathbb{C}^{N \times 1}$ is given by:

$$\mathbf{s}' = \mathbf{F}_{\mathrm{N}}^{\mathcal{H}} \mathbf{B}\, \mathbf{P}\, \mathbf{d} = \begin{bmatrix} \mathbf{s}_d \\ \mathbf{0}_{N_u \times 1} \end{bmatrix}, \tag{1}$$

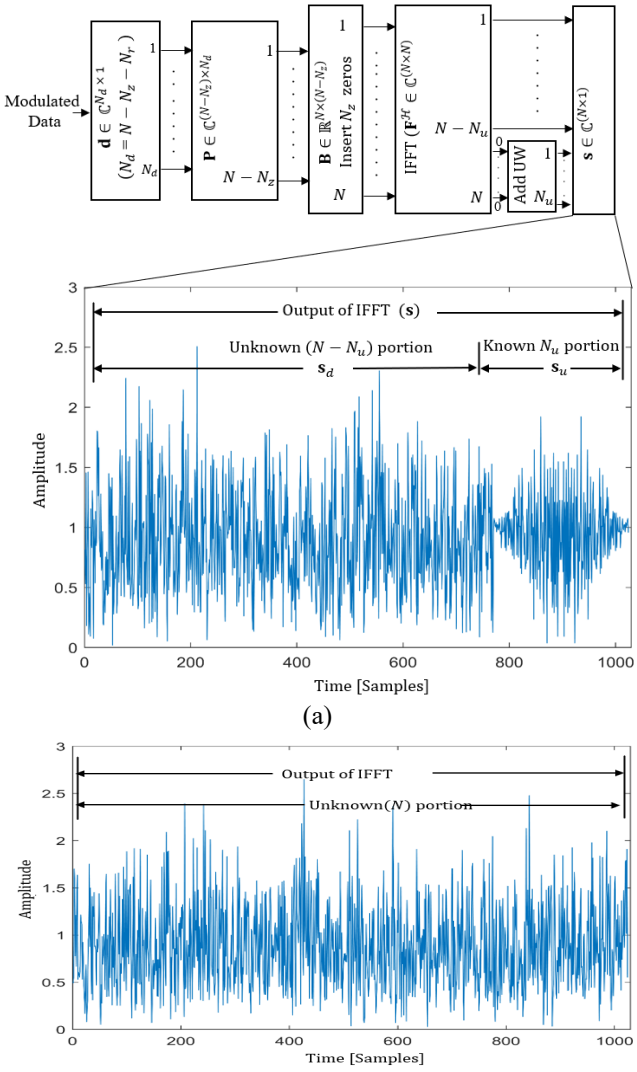

Fig. 2: OFDM blocks in the time-domain with $N = 1024$ and $N_u = 256$: (a) UW-OFDM, and (b) CP-OFDM.

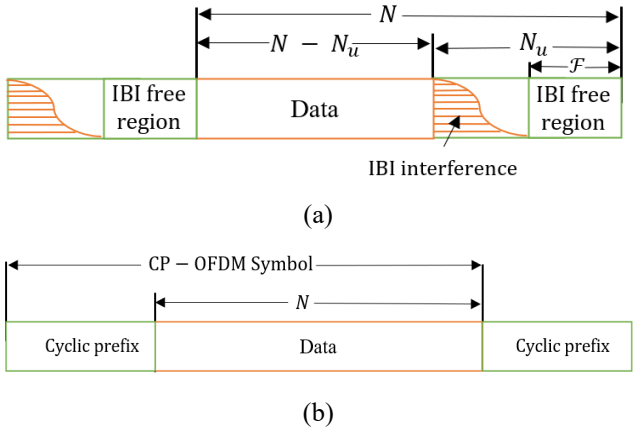

Fig. 3: Structure of the received symbol with the IBI effect of (a) the UW-OFDM symbol, and (b) the CP-OFDM symbol.

where $\mathbf{F}_{\mathrm{N}}$ is $N \times N$ DFT matrix whose (k, n)-entry is $f_{k,n} = \frac{1}{\sqrt{N}} e^{-j\frac{2\pi kn}{N}}$ for $k, n = 0,1,2,\cdots N-1$ and $j = \sqrt{-1}$, $\mathbf{B} \in$

$\mathbb{R}^{N\times(N-N_z)}$ is the mapping matrix that corresponds to a reduced version of identity matrix in which columns corresponding to the zero subcarriers are removed, $\mathbf{P} \in \mathbb{C}^{(N-N_z)\times N_d}$ is the generator matrix that will be explained shortly later, $\mathbf{d} \in \mathbb{C}^{N_d\times 1}$ is the modulated data symbols, where quadrature amplitude modulation (QAM) is adopted throughout this paper, and $(.)^{\mathcal{H}}$ is the Hermitian operator.

In the UWAC-based UW-OFDM, we use a guard interval to track the channel, so the UW sequence $\mathbf{s}_{\mathrm{u}} \in \mathbb{C}^{N_u\times 1}$ is inserted as a guard interval to avoid the inter-symbol interference (ISI) and to estimate the UWAC channel. The time-domain UW sequence is expressed as:

$$\mathbf{s}_{\mathrm{u}}(t) = \sum_{j=0}^{\mathrm{N_u}-1} \mathcal{P}_j \; e^{j2\pi j\Delta f t}, \tag{2}$$

where $\mathcal{P}$ is pseudo-noise sequence that have zero autocorrelation and constant amplitude with a constant envelope in both the time and frequency domains [24, 28] and Δf is the frequency spacing. As a result, the final time-domain signal $\mathbf{s} \in \mathbb{C}^{N\times 1}$ can be expressed as:

$$\mathbf{s} = \mathbf{s}' + \begin{bmatrix} 0_{(N-N_u)\times 1} \\ \mathbf{s}_u \end{bmatrix} = \begin{bmatrix} \mathbf{s}_{\mathrm{d}} \\ \mathbf{s}_{\mathrm{u}} \end{bmatrix}. \tag{3}$$

It's worth mentioning that, unlike TDS-OFDM [6, 16], the signal $\mathbf{s}$ will not be affected by IBI as circular convolution with the channel is experienced, and $\mathbf{s}_u$ can be subtracted in the frequency domain directly. However, this requires designing an appropriate matrix $\mathbf{P}$ that produces well-known time-domain sequences within the DFT interval as in (1).

In order to design the matrix $\mathbf{P}$, the null space approach [30] has been considered throughout this paper by dividing the $\mathbf{F}_{\mathrm{N}}^{\mathrm{H}}\mathbf{B}$ as:

$$\mathbf{F}_{\mathrm{N}}^{\mathcal{H}}\mathbf{B} = \begin{bmatrix} \mathbf{A} \\ \mathbf{Z} \end{bmatrix}, \tag{4}$$

where $\mathbf{A} \in \mathbb{C}^{(N-N_u)\times(N-N_z)}$ is the upper part, and $\mathbf{Z} \in \mathbb{C}^{N_u\times(N-N_z)}$ is the lower part. Then, in order to produce N_u zeros in (1), $\mathbf{P}$ should lie in the null space of $\mathbf{Z}$, which is equivalent to decomposing $\mathbf{P}$ as:

$$\mathbf{P} = \mathbf{Q}\mathbf{G}, \tag{5}$$

where $\mathbf{Q} \in \mathbb{C}^{(N-N_z)\times(N-N_z-N_u)}$ is equivalent to *Null*($\mathbf{Z}$) indicating the orthonormal null space basis vectors of $\mathbf{Z}$ formed by $N - N_z - N_u$ vectors, and $\mathbf{G} \in \mathbb{C}^{(N-N_z-N_u)\times(N-N_z-N_r)}$ can be chosen freely.

Therefore, the upconverted passband version of $\mathbf{s}$ in (3) can be written as:

$$\underline{\mathbf{s}}(\mathrm{t}) = \mathrm{Re}\{[\mathbf{s}(t)\mathrm{p}(t)]\, e^{2j\pi F_c t}\}, \quad t \in [0, T\,], \tag{6}$$

where $\mathrm{Re}(.)$ is the real part, $\mathrm{p}(t)$ is a rectangular pulse of duration T, where T indicates the TD-UW-OFDM symbol duration including the data and UW duration, and F_c denotes the carrier frequency. In (6), we considered filtering and pulse shaping as $\mathrm{p}(t) = 1$ for $t \in [0, T]$ and $\mathrm{p}(t) = 0$, otherwise. Also, unlike conventional OFDM, the symbol duration $T = T_d + T_g$ includes the data duration T_d and the guard interval duration T_g. As a result, the achieved data rate of UW-OFDM is similar to CP-OFDM when considering the symbol duration of both systems. The passband signal $\underline{\mathbf{s}}(\mathrm{t})$ is transmitted through UWAC channel characterized by time-varying multipath propagation and DS effect. When considering that all channel path delays share the same Doppler scaling factor α, the UWAC channel can be expressed as:

$$\mathbf{h}(t,\tau) = \sum_{l=1}^{L} A_l(t)\delta\big(\tau - (\tau_l - \alpha t)\big). \tag{7}$$

In (7), $A_l(t)$ indicates the amplitude of path l, τ_l is the l-th multipath delay component, and $\delta(.)$ is the Dirac delta function. However, when considering that each path experiences a different value of α, the UWAC in (7) can be written as:

$$\mathbf{h}(t,\tau) = \sum_{l=1}^{L} A_l(t)\delta\big(\tau - \tau_l(t)\big), \tag{8}$$

where,

$$\tau_l(t) = \tau_l + \alpha_l t. \tag{9}$$

Therefore, the received passband signal, when considering the UWAC channel given in (7), can be expressed as:

$$\underline{\mathbf{r}}(t) = \mathrm{Re}\left\{\sum_{l=1}^{L} A_l\,[\mathbf{s}(t)\;\mathrm{p}(t-\tau_l+\alpha t)]\; e^{j2\pi F_c(t-\tau_l-\alpha t)}\right\} + \underline{\boldsymbol{\nu}}(t), \tag{10}$$

where $\underline{\boldsymbol{\nu}}(t)$ represents the UWAC passband additive noise. The signal from each path of the received signal in (10) is scaled to approximately $\frac{T}{1+\alpha}$, and Doppler-induced frequency shift corresponding to $e^{j2\pi\alpha\Delta f\, t}$ occurs. This effect severely degrades the IoUT-based UWAC multicarrier modulation performance, as the orthogonality between subcarriers is lost. Two-step processing is commonly employed to overcome the DS effect, including the use of preamble and postamble sequences at the beginning and the end of every frame, respectively, to track integer DS, while the remaining residual DS, usually called the CFO effect, is handled using pilots or null subcarriers in baseband [12]. The processing of the received signal in our proposed approach employs linear frequency-modulated (LFM) segments as preamble/postamble to track the integer DS effect α' based on the lengths of the transmitted and received signals [6] as:

$$\alpha' = \frac{\Gamma}{\Gamma'} - 1, \tag{11}$$

where Γ and Γ', respectively, indicate the lengths of the transmitted and received signals. Then, $\underline{\mathbf{r}}(t)$ is resampled at $(1+\alpha')f_s$ to recover the integer DS effect, where f_s is the sampling frequency. As a result, the resampled baseband signal after being converted into discrete-time signal can be expressed as:

$$\mathbf{r}(n) \approx e^{j2\pi\frac{\alpha-\alpha'}{1+\alpha'}\times\frac{F_c}{B}} \times \sum_{l=1}^{L} A_l\, e^{-j2\pi(F_c+\,n\Delta f)\tau_l}\,\mathbf{s} + \boldsymbol{\nu}. \tag{12}$$

In (12), we assume that $\frac{1+\alpha}{1+\alpha'} = 1$ when the integer DS effect is tracked by the resampling process in (11), $\frac{\alpha-\alpha'}{1+\alpha'} F_c$ represents the residual DS effect caused by carrier frequency and subcarrier spacing mismatch and/or the relative motion between transmitting and receiving nodes, and $\mathcal{B}$ indicates the bandwidth. Therefore, the received signal $\mathbf{r}(n)$ includes the well-known time-domain guard interval sequences and the transmitted data. Unlike traditional OFDM methods, we use the time-domain guard interval in this paper to monitor the channel effects, while using all of the frequency-domain subcarriers to transmit information-bearing data.

A. Residual DS Estimation

In IoUT-based UWAC systems, estimating and compensating for the effects of multipath and DS is crucial for achieving reliable communication. However, existing OFDM methods perform this task at the expense of bandwidth efficiency, as they require the addition of components such as a time-domain guard interval to mitigate ISI and frequency-domain pilot subcarriers to track channel effects. We investigate the use of a time-domain guard interval and tracking the channel effects in order to improve the reliability of the UWAC system and enhance channel bandwidth utilization. To clarify the process of the proposed approach, let us first rewrite the signal in (12), $\mathbf{r} \in \mathbb{C}^{N\times 1}$ for one symbol, as:

$$\mathbf{r} = \mathbf{G}(\varepsilon_0)\mathbf{H}\mathbf{s} + \boldsymbol{v} = \underbrace{\mathbf{G}(\epsilon_0)\mathbf{H}\begin{bmatrix}\mathbf{s}_\mathrm{d}\\ \mathbf{s}_\mathrm{u}\end{bmatrix}}_{\mathrm{r}_0} + \boldsymbol{v}, \tag{13}$$

where $\mathbf{r}_0$ represents the noise-free received signal, $\mathbf{H}$ is an $N \times N$ circular Toeplitz matrix whose first column and first row are, respectively, given by $\left[\mathbf{h}^T,\ 0^T_{(N-L)\times 1}\right]^T$ and $\left[\mathbf{h}(0),\ 0^T_{(N-L)\times 1},\ \mathbf{h}(\mathrm{L}), \dots \mathbf{h}(1)\right]^T$. Also, given the residual DS (ε_0), which is measured in hertz (Hz), the matrix $\mathbf{G}(\epsilon_0)$ is defined as:

$$\begin{aligned}\mathbf{G}(\epsilon_0) &= \mathrm{diag}\left(1, e^{j2\pi\varepsilon_0 T_s}, \dots, e^{j2\pi\varepsilon_0 (N-1)T_s}\right)\\ &= \mathrm{diag}\left(1, e^{j\frac{\epsilon_0}{N}}, \dots, e^{j\frac{\epsilon_0}{N}(N-1)}\right).\end{aligned} \tag{14}$$

In (14), T_s is the sample interval defined as $T_s = \frac{T}{N}$, and $\epsilon_0 = \frac{2\pi\varepsilon_0}{\Delta f}$ is the normalized CFO. Therefore, given the received signal $\mathbf{r}$ and the UW $\mathbf{s}_\mathrm{u}$, our goal is to correctly detect $\mathbf{s}_\mathrm{d}$ given that ϵ_0 and CIRs ($\mathbf{h}$) are unknown.

Without the loss of the generality, we adopt the method used in [6, 16] to track ϵ_0 before estimating the CIRs. That method only utilizes the received well-defined sequences $\mathbf{s}_\mathrm{u}$. By exploiting the property of $\mathbf{r}(n) = \mathbf{r}(n+N)$, the estimated ϵ_0 can be modelled as [6, 12, 16]:

$$\hat{\epsilon_0} = \frac{\sum_{n=0}^{N_u-1} \angle(\mathrm{r}[n+N]\mathrm{r}[n]^*)}{2\pi N^2}, \tag{15}$$

where $\angle(.)$ indicates the angle of (.) in the complex plan. Therefore, the received signal in (13) can be expressed after compensating for $\hat{\epsilon}_0$ as:

$$\mathbf{y} = \mathbf{G}^{\mathcal{H}}(\hat{\varepsilon_0}) \times \mathbf{r} = \mathbf{G}^{\mathcal{H}}(\hat{\varepsilon_0})\mathbf{G}(\varepsilon_0)\mathbf{H}\begin{bmatrix}\mathbf{s}_\mathrm{d}\\ \mathbf{s}_\mathrm{u}\end{bmatrix} + \boldsymbol{v}. \tag{16}$$

In practical IoUT systems, the DS effects and channel effects, in general, cannot be estimated accurately, necessitating sophisticated approaches that are robust to these residual effects. As will be demonstrated shortly, the proposed approaches offer greater robustness to these effects compared to the currently used multicarrier schemes. In (16), when assuming the residual DS is compensated, the CIRs can be estimated and equalized using $\mathbf{y}$ in either time and/or frequency domains.

B. Channel estimation and detection

UWAC-based CS has been thoroughly tested in research to monitor the sparse channel, using various algorithms that balance complexity and performance. OMP and SOMP are among these methods and have demonstrated strong performance in tracking sparse channels [10, 11]. OMP and SOMP are commonly used schemes that provide competitive performance to track the sparse channel [16, 31, 32]. The main difference between SOMP and OMP lies in their selection strategy; the OMP selects the atomic set that best matches the residual error of a single signal, while SOMP chooses the atomic set that optimally matches the residual error of an entire signal group. To guarantee efficient performance in terms of CE, throughout this paper, we adopt SOMP for all schemes.

In this paper, we study time-domain and joint time-frequency channel estimation schemes to overcome the deterioration in bandwidth efficiency caused by the necessary overhead. To achieve this, assuming ε_0 is perfectly estimated in (16); $\mathbf{G}^{\mathcal{H}}(\hat{\varepsilon_0})\mathbf{G}(\varepsilon_0) = \boldsymbol{I}_N$ where $\boldsymbol{I}_N$ is $N \times N$ identity matrix. Thus, the received $\mathbf{s}_\mathrm{u}$ can be extracted from the received signal as:

$$\mathbf{y}_\mathrm{u} = \mathbf{H}_\mathrm{u}\mathbf{s}_\mathrm{u} + \boldsymbol{v}_\mathrm{u}, \tag{17}$$

where $\mathbf{y}_\mathrm{u} \in \mathbb{C}^{N_u\times 1}$ is the last N_u samples of y, $\mathbf{H}_\mathrm{u} \in \mathbb{C}^{N_u\times N_u}$ is the portion of the channel matrix $\mathbf{H}$ that affects the $\mathbf{r}_\mathrm{u}$,$\boldsymbol{v}_\mathrm{u} \in \mathbb{C}^{N_u\times 1}$ is the additive noise. Generally, the guard interval in multicarrier modulation is chosen to be longer than the maximum channel delay; $N_u >> L$. Inspired by the characteristics of the circular Toeplitz matrix $\mathbf{H}$ which is constructed from the sparse channel vector $\mathbf{h} \in \mathbb{C}^{L\times 1}$, (17) can, alternatively, be written as:

$$\mathbf{y}_\mathrm{u} = \boldsymbol{\Psi}\mathbf{h} + \boldsymbol{v}_\mathrm{u}, \tag{18}$$

where $\boldsymbol{\Psi} \in \mathbb{C}^{N_u\times N_u}$ is built using $\mathbf{s}_\mathrm{d}$ and $\mathbf{s}_\mathrm{u}$ as:

$$\boldsymbol{\Psi} = \begin{bmatrix} \mathrm{s}_{\mathrm{u},0} & \mathrm{s}_{\mathrm{d},N_d-1} & \cdots & \mathrm{s}_{\mathrm{d},N_d-L+1} \\ \mathrm{s}_{\mathrm{u}.1} & \mathrm{s}_{\mathrm{u},0} & \cdots & \mathrm{s}_{\mathrm{d},N_d-L+2} \\ \vdots & \vdots & \ddots & \vdots \\ \mathrm{s}_{\mathrm{u},L-1} & \mathrm{s}_{\mathrm{u},L-2} & \cdots & \mathrm{s}_{\mathrm{u},0} \\ \mathrm{s}_{\mathrm{u},,L} & \mathrm{s}_{\mathrm{u},L-1} & \cdots & \mathrm{s}_{\mathrm{u},1} \\ \vdots & \vdots & \ddots & \vdots \\ \mathrm{s}_{\mathrm{u},N_u-1} & \mathrm{s}_{\mathrm{u},N_u-2} & \cdots & \mathrm{s}_{\mathrm{u},N_u-L} \end{bmatrix}. \tag{19}$$

The IBI shown in (19) is similar to that previously described in Fig. 3. For example, the rows that include a portion of $\mathbf{s}_d$ represent the guard interval affected by IBI, while the lower rows indicate the IBI-free region. In order to guarantee accurate channel estimation, the length of the IBI-free region ($\mathcal{F}$) must be greater than L. Therefore, CS-based channel estimate can be achieved using the IBI-free region $\boldsymbol{\Phi} \in \mathbb{C}^{\mathcal{F}\times L}$ extracted from $\boldsymbol{\Psi}$ in (19) as:

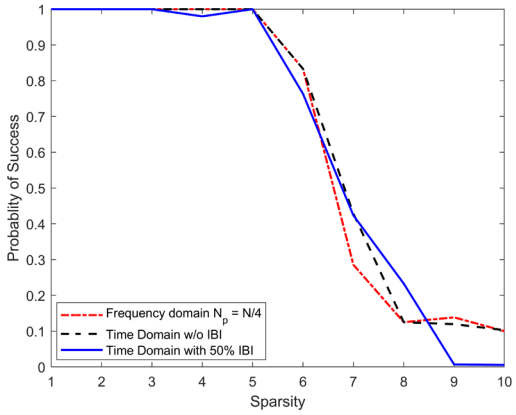

Fig. 4: Success probability estimation of UWAC sparsity with $N = 1024, L = 128$ for 10^4 trials of the experiment.

$$\mathbf{\Phi} = \begin{bmatrix} s_{u,L-1} & s_{u,L-2} & \cdots & s_{u,0} \\ s_{u,,L} & s_{u,L-1} & \cdots & s_{u,1} \\ \vdots & \vdots & \ddots & \vdots \\ s_{u,N_u-1} & s_{u,N_u-2} & \cdots & s_{u,N_u-L} \end{bmatrix}. \quad (20)$$

Without loss of the generality, SOMP [16, 32] has been employed to estimate the CIRs of the UWAC channel based on the IBI-free part $\mathbf{y}_{\mathcal{F}}$ extracted from the signal in (17) as:

$$\mathbf{y}_{\mathcal{F}} = \mathbf{\Phi h} + \boldsymbol{v}_{\mathcal{F}}. \quad (21)$$

The thresholding method described in [11] can be applied to remove the channel coefficients that fall below a specific threshold. Throughout this paper, we assume that the channel coefficients with $|h| < 0.15$ are removed. Subsequently, by ignoring the effect of the noise in (16) for simplicity, the channel equalization can be performed in the frequency domain as:

$$\bar{\mathbf{s}} = \boldsymbol{g}\mathbf{F}_N \mathbf{y} = \boldsymbol{g}\left(\mathbf{P}\,\mathbf{d} + \mathbf{F}_N \begin{bmatrix} \mathbf{0}_{(N-N_u)\times 1} \\ \mathbf{s}_u \end{bmatrix}\right), \quad (22)$$

where $\boldsymbol{g}$ is the minimum mean square error (MMSE) equalizer using the estimated CIRs $\hat{\mathbf{h}}$ and the $N \times N$ channel frequency response matrix $\mathbf{\Theta}$ whose $(u+1, v+1)$-entry $\mathbf{\Theta}_{u,v}$ is given by [33]:

$$\mathbf{\Theta}_{u,v} = \sum_{l=0}^{L-1}\left(\frac{1}{N}\sum_{n=0}^{N-1}\mathbf{h}_{n,l}\, e^{-\frac{j2\pi n(u-v)}{N}}\right) e^{-\frac{j2\pi v n l}{N}}. \quad (23)$$

When considering the channel to be constant within the symbol duration, the inter-carrier interference (ICI) will be zero; this implies $u = v$, and $\mathbf{\Theta}$ is a diagonal matrix. Therefore, $\boldsymbol{g}$ can be expressed as:

$$\boldsymbol{g} = (\mathbf{\Theta}^{\mathcal{H}}\mathbf{\Theta} + \frac{1}{\gamma}\mathbf{I}_N)^{-1}\mathbf{\Theta}^{\mathcal{H}}, \quad (24)$$

where γ is the signal-to-noise ratio (SNR) per symbol. Finally, the estimated modulated data $\hat{\mathbf{d}}$ can be extracted by applying $\mathbf{P}^{\mathcal{H}}$, since $\mathbf{P}$ is a unitary matrix, as follows:

$$\hat{\mathbf{d}} = \mathbf{P}^{\mathcal{H}}\left(\bar{\mathbf{s}} - \mathbf{F}_N \begin{bmatrix} 0_{(N-N_u)\times 1} \\ \mathbf{s}_u \end{bmatrix}\right). \quad (25)$$

Based on (25), it is clear that UW-OFDM differs from TDS-OFDM [16, 24] in that it overcomes the IBI by smoothly removing the inserted UW in the frequency domain. Therefore, it is possible to achieve an efficient UWAC system. However, this is achieved at the cost of guaranteeing the IBI-free region in (20) which can only be ensured by using a longer time-domain guard interval, i.e., $N_u \geq 2L$ or $\mathcal{F} \geq L$. In practical scenarios, L cannot be predicted, and using longer N_u reduces the spectral efficiency. Also, sensitivity to higher residual DS is increased. To address these issues and to enable efficient CE approach without compromising subcarrier utilization, we present TFCE-UW-OFDM, which utilizes only 3.1% of the frequency-domain subcarriers to efficiently track the CIRs coefficients.

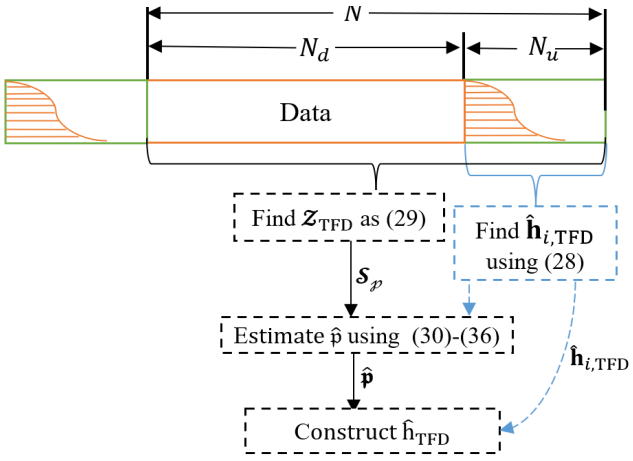

Fig. 5: TFCE-UW-OFDM channel estimation procedure

III. UWAC-BASED TFCE-UW-OFDM SYSTEM MODEL

Practically, it is not feasible to always guarantee that $\mathcal{F} \geq L$ in (20) as the maximum channel delay cannot be predicted. As a result, the channel delay coefficients cannot be accurately estimated. However, based on our analyzing, we find the sparsity of the channel can be correctly estimated even under IBI effect due to the unique autocorrelation properties of $\mathbf{s}_u$. To demonstrate this, we calculated the probability of success ($\wp$) numerically, as shown in Fig. 4 using different levels of sparsity and 10^4 trials at SNR = 10dB. For example, we compute the likelihood that sparse channel estimation algorithm accurately identifies the important channel taps (the positions where the impulse response has non-zero values) based on a specific level of sparsity. Then $\wp$ is calculated with respect to total number of trials [34]. We chose to detect a maximum of 15 channel taps. As shown in Fig. 4, the probability of identifying the correct sparsity is approximately the same in IBI-free regions as it is in the frequency domain, and/or when using the IBI-free region, even though IBI affects 50% of the IBI-free regions due to channel delay. Consequently, only the channel delay coefficients need to be estimated to achieve a reliable UWAC system. Additionally, we will show later in this paper that TD-based CE has worse performance compared to the proposed frequency-domain approach in the presence of a residual DS effect. Therefore, to tackle that issue, we present joint time-frequency CE-based UW-OFDM.

Fig. 5 shows the CE process achieved by TFCE-UW-OFDM. Unlike the TD-UW-OFDM transmitted signal described in (1), frequency-domain pilots are inserted, resulting in the time-domain TFCE-UW-OFDM signal $\mathbf{s}'_{TFD} \in \mathbb{C}^{N\times 1}$ to be:

$$\mathbf{s}'_{\mathrm{TFCE}} = \mathbf{F}_{\mathrm{N}}^{\mathcal{H}}\mathbf{B}\,\mathbf{P}\,\mathbf{d} + \mathbf{F}_{\mathcal{p}}^{\mathcal{H}}\boldsymbol{\mathcal{p}} = \begin{bmatrix}\mathbf{s}_d \\ \mathbf{n}_{N_u\times 1}\end{bmatrix}. \quad (26)$$

In (26), it is worth noting that although the same procedure described in Fig. 2 can be straightforwardly generalized to generate $\mathbf{s}'_{\mathrm{TFCE}}$, the dimensions of the matrices involved mainly depend on the input vectors $\mathbf{d}$ and $\boldsymbol{\mathcal{p}}$, since $N_{\mathcal{p}}$ out of N_d subcarriers are allocated for carrying the pilot sequences. Specifically, in contrast to the TD-UW-OFDM approach, the input vectors and matrices are defined as follows: $\mathbf{d} \in \mathbb{C}^{(N_d-N_{\mathcal{p}})\times 1}$, $\mathbf{P} \in \mathbb{C}^{(N-N_z-N_{\mathcal{p}})\times(N_d-N_{\mathcal{p}})}$, and $\mathbf{B} \in \mathbb{R}^{N\times(N-N_z-N_{\mathcal{p}})}$. The resulting time-domain vector is then added to a known vector produced by $\mathbf{F}_{\mathcal{p}}^{\mathcal{H}}\boldsymbol{\mathcal{p}}$. For simplicity, the additive effect of this operation on the vector $\mathbf{s}_d$ is ignored in the current formulation. Also, $\mathbf{F}_{\mathcal{p}}^{\mathcal{H}} \in \mathbb{C}^{N\times N_{\mathcal{p}}}$ and $\mathbf{n}_{N_u\times 1}$, respectively, indicate the $N_{\mathcal{p}}$ columns in the matrix $\mathbf{F}_{\mathrm{N}}^{\mathcal{H}}$ multiplied with the pilot vector $\boldsymbol{\mathcal{p}} \in \mathbb{R}^{N_{\mathcal{p}}\times 1}$, and the lower part of $\mathbf{s}'_{\mathrm{TFCE}}$ resulted time-domain guard interval from $\mathbf{F}_{\mathcal{p}}^{\mathcal{H}}\boldsymbol{\mathcal{p}}$. It's important to clarify that $\boldsymbol{\mathcal{p}}$ is a well-known vector and the resulted $\mathbf{n}_{N_u\times 1}$ will also be known and can be optimized to be minimum, and similar procedure followed in (4)-(5) can also be directly deployed to derive $\mathbf{P}$. However, even if it's not zero, that does not affect the performance as we will show in Section V. Moreover, $N_{\mathcal{p}}$ does not need to be longer than the channel delay L as in the conventional approaches, but it should be greater than the detected channel sparsity. The final time-domain signal $\mathbf{s}_{\mathrm{TFCE}} \in \mathbb{C}^{N\times 1}$ equivalent to (3) is given by:

$$\mathbf{s}_{\mathrm{TFCE}} = \mathbf{s}'_{\mathrm{TFCE}} + \begin{bmatrix}0_{(N-N_u)\times 1} \\ \mathbf{s}_u\end{bmatrix} = \begin{bmatrix}\mathbf{s}_d \\ \mathbf{n}+\mathbf{s}_u\end{bmatrix}. \quad (27)$$

Then, the same procedure is followed with the TFCE-UW-OFDM, taking into account the dimensions of the transmitted signals due to the insertion of the pilot vector $\boldsymbol{\mathcal{p}}$. However, the CIRs are not estimated only in the time domain, but in both time and frequency domains. To this end, the sparsity of the channel is detected first using the same process in (18) as:

$$\mathbf{y}_{u,\mathrm{TFCE}} = \boldsymbol{\Psi}_{\mathrm{TFCE}}\mathbf{h} + \boldsymbol{\mathcal{v}}_{u,\mathrm{TFCE}}, \quad (28)$$

where the measurement matrix $\boldsymbol{\Psi}_{\mathrm{TFCE}}$ is constructed using the received $\mathbf{s}_{\mathrm{u,TFCE}} = \mathbf{n}+\mathbf{s}_{\mathrm{u}}$ by the same process in (18), and $\boldsymbol{\mathcal{v}}_{u,\mathrm{TFCE}}$ is the AWGN. As mentioned earlier, the IBI-free region $(\mathcal{F})$ is considered to be unavailable as it cannot be guaranteed in the practical UWAC systems, and the channel sparsity can be detected using the whole guard interval as demonstrated in Fig. 4. Therefore, the sparsity of UWAC channel is first detected using SOMP algorithm; assuming we have detected χ non-zero channel values. Although the channel delay can be detected correctly as demonstrated previously in Fig. 4, the channel coefficients are still affected by IBI. So, to track the channel coefficients correctly, we employ the pilot vector $\boldsymbol{\mathcal{p}}$ in the frequency domain. It's worth mentioning that the pilot length $N_{\mathcal{p}}$ only needs to be greater than the channel sparsity; $N_{\mathcal{p}} > \chi$, which is different from the conventional approaches which should be longer than the channel delay L to guarantee precise CE. Let us denote the initial estimated channel as $\hat{\mathbf{h}}_{i,\mathrm{TFCE}}$; the frequency-domain TFCE-UW-OFDM received signal $\boldsymbol{\mathcal{S}} \in \mathbb{C}^{N\times 1}$ can be written using (23) as:

Table 1: System parameters

System parameter	OFDM	UW-OFDM
Symbol duration T (ms)	170.7	170.7
Guard duration T_g (ms)	42.7	-
Total symbol duration (ms)	213.4	170.7
Number of subcarriers N	1024	1024
Pilot length $N_{\mathcal{p}}$	256	32
Number of redundant subcarrier (N_r)	-	256
Length of guard interval (N_u)	-	256
Bandwidth $\mathcal{B}$ (KHz)	6	6
Sampling frequency f_s (KHz)	96	96
Carrier frequency F_c (KHz)	13	13
Subcarrier spacing Δf (Hz)	5.86	5.86
Doppler shift effect (Hz)	0.3	0.3
Modulation order M	QPSK	QPSK
Channel delay (ms)	22	22
Roll-off factor $\mathrm{p}(t)$	0.65	0.65
Channel Coding Rate	1/2	1/2

$$\boldsymbol{\mathcal{S}} = \boldsymbol{\Theta}\underbrace{\mathbf{F}_N\,\mathbf{s}_{\mathrm{TFCE}}}_{\mathcal{Z}_{\mathrm{TFCE}}} = \boldsymbol{\Theta}\mathbf{F}_N^{\mathcal{H}}\begin{bmatrix}\mathbf{s}_d \\ \mathbf{n}+\mathbf{s}_u\end{bmatrix}, \quad (29)$$

where $\boldsymbol{\mathcal{Z}}_{\mathrm{TFCE}}$ is the frequency-domain transmitted signal. Let the inserted pilot vector $\boldsymbol{\mathcal{p}}$ in the frequency domain, be denoted as $\boldsymbol{\mathcal{S}}_{\mathcal{p}}$ that results a well-known data modelled as the summation of the inserted $\boldsymbol{\mathcal{p}}$ and $\mathbf{F}_{\mathrm{N}}\begin{bmatrix}0 \\ \mathbf{n}+\mathbf{s}_{\mathrm{u}}\end{bmatrix}$. So, the non-zero path coefficients in $\hat{\mathbf{h}}_{i,\mathrm{TFCE}}$ can be modeled by $\mathcal{Q}$-order Taylor series expansion as [35]:

$$\mathrm{h}_{n,l} = \mathbf{q}_n\mathbf{p}_l + \mathfrak{d}_{n,l}, \quad (30)$$

where $\mathbf{q}_n = [1\ n\ n^2 \dots n^{\mathcal{Q}}]_{1\times(\mathcal{Q}+1)}$, $\mathfrak{d}_{n,l}$ is the modelling approximation error, and $\mathbf{p}_l = [\mathrm{p}_{l,0}\ \mathrm{p}_{l,1} \dots \mathrm{p}_{l,\mathcal{Q}}]_{(\mathcal{Q}+1)\times 1}$ whose $\mathbf{p}_{l,q}$-entry is the polynomial coefficient. Accordingly, using (23) and (29), the received frequency-domain signal on the k-th subcarrier, assuming that ICI is negligible when $|u-v| > d$, where d is the number of adjacent subcarriers affected by the ICI, can be written as:

$$\begin{aligned}\boldsymbol{\mathcal{S}}_k &= \boldsymbol{\Theta}_{k,k}\,\boldsymbol{\mathcal{Z}}_{\mathrm{TFCE},k} + \sum_{j=0,j\neq k}^{N-1}\boldsymbol{\Theta}_{k,j}\,\boldsymbol{\mathcal{Z}}_{\mathrm{TFCE},j} + \boldsymbol{V}_{\mathrm{TFCE},k} \\ &\approx \sum_{n=0}^{N-1}\sum_{l=0}^{L-1}\sum_{q=0}^{\mathcal{Q}}\mathbf{p}_{l,q}n^q\boldsymbol{\lambda}_{n,l,k} + \underbrace{\sum_{n=0}^{N-1}\sum_{l=0}^{L-1}\mathfrak{d}_{n,l}\boldsymbol{\lambda}_{n,l,k} + \boldsymbol{V}_{\mathrm{TFCE},k}}_{\boldsymbol{\varsigma}_k}\end{aligned} \quad (31)$$

where,

$$\boldsymbol{\lambda}_{n,l,k} = \frac{1}{N}\sum_{q=0}^{\mathcal{Q}} e^{-\frac{j2\pi n(k-d)}{N}}e^{-\frac{j2\pi qnl}{N}}\boldsymbol{\mathcal{Z}}_{\mathrm{TFCE},q}, \quad (32)$$

and $\boldsymbol{V}_{\mathrm{TFCE}} = \mathbf{F}_N^{\mathcal{H}}\,\boldsymbol{\mathcal{v}}_{\mathrm{TFCE}}$. Alternatively, $\boldsymbol{\mathcal{S}}_k$ can be rewritten as:

$$\boldsymbol{\mathcal{S}}_k = \boldsymbol{\Lambda}_k\mathbf{q}\mathbf{p} + \boldsymbol{\varsigma}_k, \quad (33)$$

where,

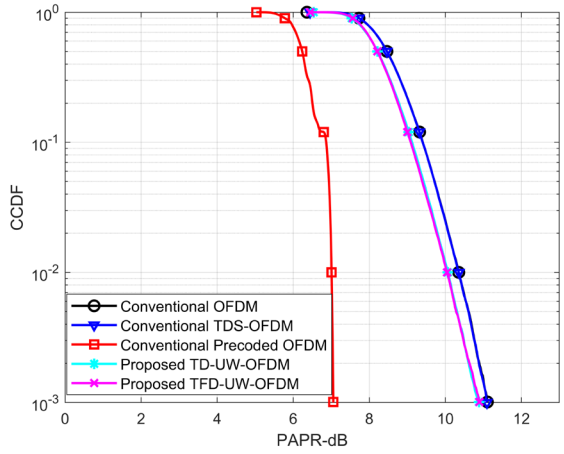

Fig. 6: PAPR performance comparison.

$$\boldsymbol{\Lambda}_k = \left[\boldsymbol{\lambda}_{0,0,k} \ \dots \ \boldsymbol{\lambda}_{0,\chi-1,k} \ \dots \ \boldsymbol{\lambda}_{N-1,0\chi-1k}\right]_{1\times\chi N},$$

$$\mathbf{q} = \left[\text{diag}\{\mathbf{q}_0^T \ \mathbf{q}_1^T \ \dots \ \mathbf{q}_{N-1}^T\}\right]_{\chi\times(Q+1)\chi},$$

$$\mathbf{p} = \left[\mathbf{p}_0 \ \mathbf{p}_1 \ \dots, \mathbf{p}_{\chi-1}\right]_{(Q+1)\chi\times 1}. \quad (34)$$

Therefore, the received frequency-domain pilot vector can be written as:

$$\boldsymbol{\mathcal{S}}_p = \boldsymbol{\Lambda}\mathbf{q}\mathbf{p} + \boldsymbol{\xi}, \quad (35)$$

and $\mathbf{p}$ can be estimated using MMSE criterion [36] as:

$$\hat{\mathbf{p}} = (\boldsymbol{\Lambda}\mathbf{q})^{\dagger}\boldsymbol{\mathcal{S}}_p = \left((\boldsymbol{\Lambda}\mathbf{q})^{\mathcal{H}}(\boldsymbol{\Lambda}\mathbf{q}) + \frac{1}{\gamma}\mathbf{I}_{(Q+1)\chi}\right)^{-1}(\boldsymbol{\Lambda}\mathbf{q})^{\mathcal{H}}\boldsymbol{\mathcal{S}}_p, \quad (36)$$

where $(.)^{\dagger}$ denotes the Moore-Penrose inverse matrix, and $\frac{1}{\gamma}$ can be obtained using $\mathbf{s}_{u,\text{TFCE}}$ via a time-domain estimator [37]. As a result, the estimated $\hat{\mathbf{h}}_{\text{TFCE}}$ can be constructed, and $\boldsymbol{\Theta}$ in (29) will be known. The equalization and detection process can then be carried out straightforwardly, similar to TD-UW-OFDM explained in Section II.B.

IV. Performance Analysis

This section studies the performance of the proposed approaches in terms of PAPR, bandwidth efficiency, and required computational complexity, using the parameters shown in Table 1.

A. PAPR Performance

The PAPR is one of the main issues affecting the performance of OFDM approaches due to the superposition of a large number of symbols at the transmitter side [6]. Unlike conventional OFDM, the PAPR of TD-UW-OFDM should be calculated over the entire time-domain signal, including the added time-domain guard interval $\mathbf{s}_u$. By using (3), the PAPR of the TD-UW-OFDM approach is given by:

$$\text{PAPR}_{\text{TD-UW-OFDM}} = \frac{\max\limits_{0\le n\le N-1}|\mathbf{s}_n|^2}{E[|\boldsymbol{s}_n|^2]}, \quad (37)$$

where $\max\limits_{0\le n\le N-1}$ and $E[|.|^2]$, respectively denote the maximum instantaneous power and the average signal power. On the other hand, the PAPR of the TFCE-UW-OFDM approach can be expressed using (27), as:

$$\text{PAPR}_{\text{TFCE-UW-OFDM}} = \frac{\max\limits_{0\le n\le N-1}\left|\mathbf{s}_{\text{TFCE},n}\right|^2}{E\left[\left|\boldsymbol{s}_{\text{TFCE},n}\right|^2\right]}. \quad (38)$$

It's worth mentioning that, unlike conventional precoded OFDM approaches [6, 14], where a unitary precoding matrix is used to cancel the effect of the DFT matrix and reduce the PAPR, the generator matrix **P** does not reduce the PAPR of UW-OFDM systems. Instead, it is utilized to enforce the time-domain guard interval to be known. Particularly, the time-domain guard interval is enforced by be zero during the optimization in (3). As a result, the PAPR effect increases since $E[|\boldsymbol{s}_n|^2]$ in (37) is decreased. On the other hand, when adding the known UW in (27), the mean of the time-domain signal will be increased leading to a small reduction in the PAPR. Therefore, as shown in Fig. 6, using the complementary cumulative distribution function (CCDF), the PAPR performance of the proposed approaches slightly outperforms that of conventional UWAC-OFDM [38], and TDS-OFDM [16] while the precoded UWAC-OFDM [14] offers up to 3 dB better PAPR performance at the cost of higher sensitivity to the DS effect, as demonstrated later in Section V.A.

B. Spectral and Energy Efficiency Performance

Generally, pilot symbols are utilized in IoUT-based UWAC systems to track the channel effects and ensure reliable transmission. For example, a guard interval is utilized in OFDM to prevent the ISI while pilot data is used to estimate/equalize the channel. This dedicated overhead required to compensate for channel effects dramatically affects the channel utilization. The subcarriers utilizations $\mathscr{b}_{eff}$ and energy efficiency e_{eff} are exploited in this paper to analyze the spectral and energy efficiency of the proposed approaches. The $\mathscr{b}_{eff}$ and e_{eff} of the presented approaches are given as follows [6]:

$$\mathscr{b}_{eff} = \frac{N_d}{N_d + N_p} \times \frac{N}{N_d + N_u} \times 100\%, \quad (39)$$

and

$$e_{eff} = \frac{N_d}{N_d + b^2 N_p} \times \frac{N}{N_d + a^2 N_u} \times 100\%, \quad (40)$$

where N_p, b and a, respectively denote the number of pilot subcarriers, the amplitude of the inserted frequency-domain pilots and the time-domain guard interval.

C. Computational Complexity Analysis

To ensure a fair comparison, the same channel estimator and equalizer have been used for the proposed schemes as well as with conventional UWAC OFDM. Therefore, the computational complexity is investigated at the transmitter side, of each scheme in terms of the required transforms, while at the receiver side in terms of transforms, channel estimation and channel equalization. The comparison is made against the conventional CP-OFDM since the TDS-OFDM and UW-OFDM require similar computational complexity to the CP-OFDM and TD-UW-OFDM, respectively.

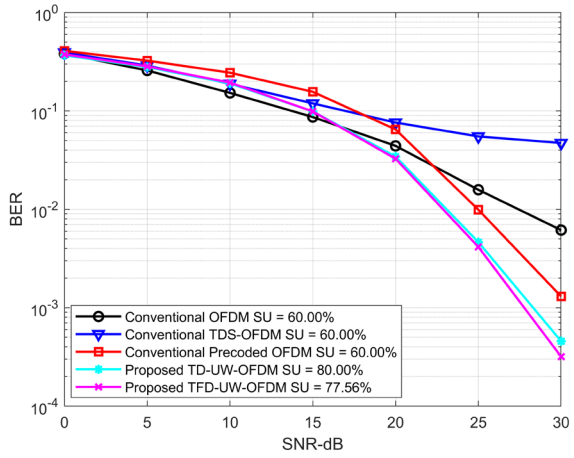

Fig. 7: BER performance comparison with different subcarrier utilization.

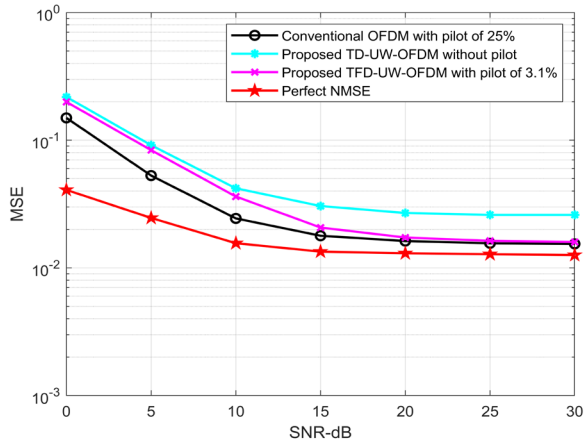

Fig. 8: MSE performance comparison.

At the transmitting end, all schemes require to perform IFFT processing with complexity of $\mathcal{O}\left(\frac{N}{2}\log_2 N\right)$, but the proposed TD-UW-OFDM and TFCE-UW-OFDM require additional $\mathcal{O}(N \times N_d)$ complexity when multiplying with the matric **P** in (1). Similarly, the transformation procedure at the receiving end is also increased in TD-UW-OFDM and TFCE-UW-OFDM by $\mathcal{O}(N \times N_d)$ compared to conventional CP-OFDM and TDS-OFDM. In terms of channel estimation, assuming all schemes use the same size of measurement matrix in (20), the resulted computational complexity to detect χ paths is $\mathcal{O}(\chi \mathcal{F} L)$ for all schemes. However, the frequency-domain channel tracking in the proposed TFCE-UW-OFDM needs higher computation complexity. For instance, calculating $(\mathbf{\Lambda q})^{\dagger}$ in (34) needs $2N_p(Q+1)^2\chi^2 + (Q+1)^3\chi^3$ times of multiplication and $N_p(Q+1)\chi$ times of multiplication are needed for the matrix multiplication [23]. As mentioned earlier, the number of significant pats χ is not high due to the nature of UWAC leading to decreasing the required length of frequency-domain pilot N_p, thereby mitigating the potential explosion of the overall computational complexity. Finally, the procedure for performing the channel equalization needs the same algorithm which is SOMP with required complexity of $\mathcal{O}(N)$ to perform the MMSE equalization for all schemes. It is straightforward to observe that, although the proposed approaches involve higher computational complexity, it remains manageable and practical, as they do not require large-scale matrix inversion or matrix–matrix multiplication especially when compared to the conventional UW-OFDM approach [25].

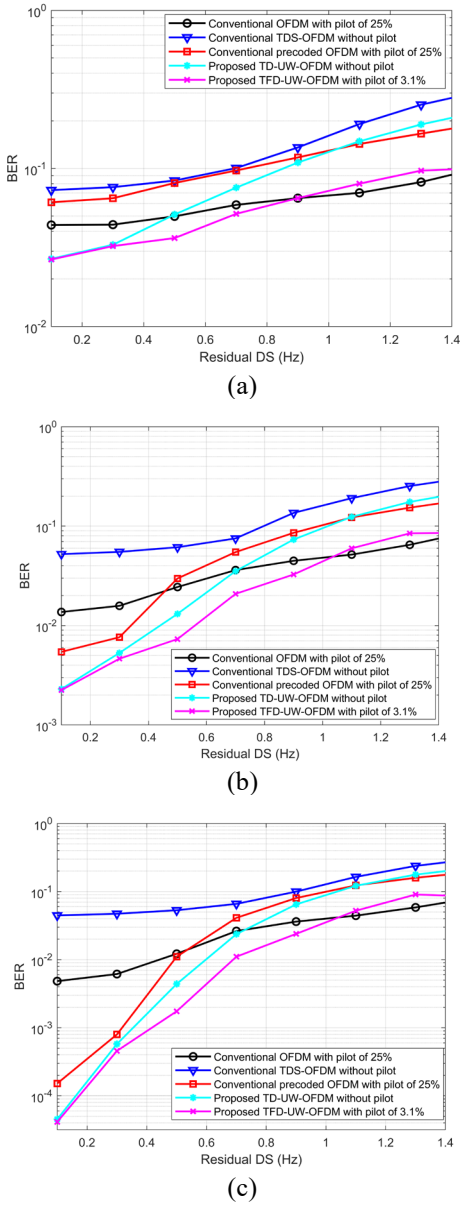

Fig. 9: BER performance comparison at different DS effects at (a) SNR=20dB, (b) SNR=25dB and (c) SNR=30dB.

V. Simulation And Experimental Results

In order to ensure the feasibility of the proposed approaches and confirm their superior performance for IoUT-based UWAC system, this section investigates the performance compares the results against the conventional UWAC-OFDM [38], TDS-OFDM [16], and precoded UWAC-OFDM [14]. The performance is investigated using simulation and experimental tests conducted in Zhoushan, China with a distance of 300 meters.

A. Simulation Results

Table 1 displays the system parameters used throughout this paper. In order to ensure a fair comparison, all systems are implemented under similar conditions, although the TD-UW-OFDM and TFCE-UW-OFDM do not require a guard interval outside the DFT interval. As a result, the total symbol duration varies between systems. In simulation, all schemes utilized the statistical UWAC channel described in [39], assuming single-input single-output (SISO) system, with both transmitter and receiver placed 4 meters below the water surface and separated by 1 kilometer.

The maximum number of sparsity to be estimated is set to $\chi = 10$. The DS effect is set to be 0.3 Hz except in figures where it is varied to evaluate robustness to residual DS. TD-UW-OFDM and regular TDS-OFDM use the time-domain guard interval to estimate the channel, while TFCE-UW-OFDM uses 32 additional pilot subcarriers to monitor the channel effect in the frequency domain. This value represents only 3.1% of the total available number of subcarriers, whereas conventional and precoded OFDM schemes use 256 pilot subcarriers, representing 25% of the available subcarriers, to track the channel effects. In the experimental tests, null-subcarrier-based residual DS estimation is applied to all schemes. The remaining parameters are listed in Table 1, where it's shown that the smaller required pilot overhead N_p significantly boosts the overall data rate. Although UW-OFDM and CP-OFDM differ in their symbol durations, they achieve similar overall data rate when using comparable guard intervals and pilot overheads [29]. Based on the parameters in Table 1, and ignoring channel coding, the total achievable data rate of conventional UWAC-OFDM, is 7.2 kbps, while the proposed TD-UW-OFDM and TCE-UW-OFDM reach 9.3 kbps and 9.6 kbps, respectively. Additionally, both conventional UW-OFDM and TDS-OFDM attain the same data rate as TD-UW-OFDM because they do not require any additional N_p in the frequency domain to track channel effects.

Fig. 7 shows the bit error rate (BER) performance comparison. As shown the proposed TD-UW-OFDM and TFCE-UW-OFDM outperform conventional OFDM by up to 5 dB at SNR = 25 dB. In contrast, TDS-OFDM is severely affected by IBI, as subtracting it in harsh UWAC channels becomes a highly challenging. Also, the proposed methods outperform the precoded OFDM, even though the precoder matrix provides more diversity and the huge pilot vector used in the precoded OFDM tracks the channel effect. However, the performance of precoded OFDM degrades due to its sensitivity to DS [40], particularly at lower SNR levels. The performance gain of the proposed approaches is further supported by higher subcarrier utilization, as shown in Table 2, where the proposed approaches can meaningfully improve the subcarrier utilization with better BER performance. It's worth mentioning that the conventional UW-OFDM achieves similar subcarrier utilization as TDS-OFDM and TD-UW-OFDM. The two proposed approaches almost offer identical BER performance since we provided a longer IBI-free region than the channel delay L. In fact, that is advantageous to the UWAC systems since the bandwidth efficiency is considered as the main problem in that environment. On the other hand, the normalized mean square error (NMSE) corresponding to the same conditions used in Fig. 7 is shown in Fig. 8. NMSE is defined as follows:

Table 2: Comparison of Subcarriers Utilization.

N_{CP}	DFT-OFDM [36]	TDS-OFDM [16]	TD-UW-OFDM	TFCE-UW-OFDM
$N/4$	60.00%	80.00%	80.00%	77.56%
$N/8$	77.78%	88.89%	88.89%	86.18%
$N/16$	88.23%	94.12%	94.12%	91.26%

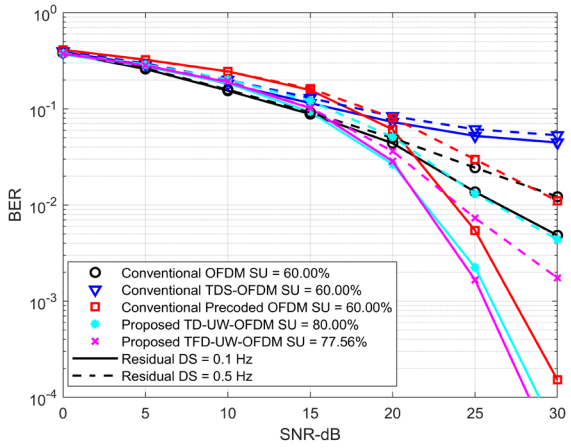

Fig. 10: BER performance comparison at different ε_0 and subcarrier utilization.

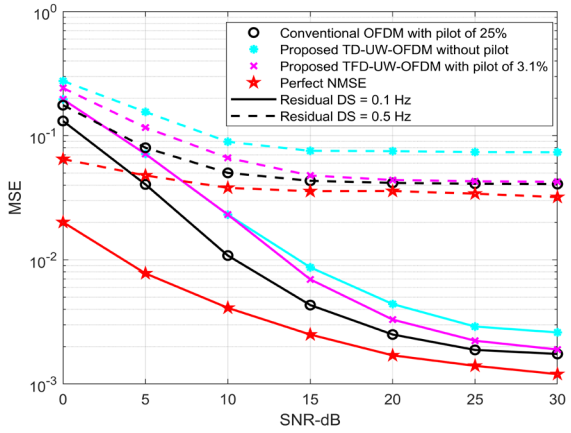

Fig. 11: MSE performance comparison at different ε_0.

$$\text{NMSE} = \frac{E\left\{\left|\mathrm{h}_l - \hat{h}_l\right|^2\right\}}{E\{|\mathrm{h}_l|^2\}}. \tag{41}$$

As TDS-OFDM and precoded OFDM show similar NMSE to TD-UW-OFDM and conventional OFDM, respectively, they are omitted from Fig. 8 for clarity. The perfect NMSE, used as a reference in that comparison, is produced by using the full data, including modulated data and pilot vectors, for tracking the channel effects. As demonstrated, the utilization of huge pilot data improves the frequency-domain CE's NMSE performance. The proposed approaches still provide better BER performance due to the integration of the guard within the DFT interval.

To further investigate the robustness of the proposed approaches to the UWAC environment effects, the BER performance against different DS values is shown in Fig. 9 at SNRs of 20, 25, and 30 dB. Fig. 9 demonstrates that the proposed approaches maintain excellent BER performance under increasing DS. However, at a DS that is higher than 1 Hz,

Table 3: Comparison of experimental test BER performance

#	OFDM [38]		TDS-OFDM [16]		Precoded-OFDM [14]		TD-UW-OFDM		TFCE-UW-OFDM	
	Coded	Uncoded	Coded	Uncoded	Coded	Uncoded	Coded	Uncoded	Coded	Uncoded
1	7.54×10^{-4}	0.12	4.33×10^{-3}	0.22	4.11×10^{-4}	0.26	3.72×10^{-4}	0.18	2.19×10^{-4}	0.011
2	0	0.095	9.71×10^{-3}	0.18	0	0.012	0	0.035	0	0.015
3	8.13×10^{-4}	0.22	8.21×10^{-4}	0.34	0	0.054	2.24×10^{-4}	0.084	0	0.02
4	8.13×10^{-4}	0.34	9.66×10^{-3}	0.3	3.87×10^{-4}	0.11	3.21×10^{-4}	0.15	3.21×10^{-4}	0.087
5	2.93×10^{-4}	0.098	5.83×10^{-3}	0.22	4.35×10^{-4}	0.17	0	0.082	0	0.015
Average	5.35×10^{-4}	0.1746	6.07×10^{-3}	0.252	2.47×10^{-4}	0.1212	1.83×10^{-4}	0.1062	1.08×10^{-4}	0.0428

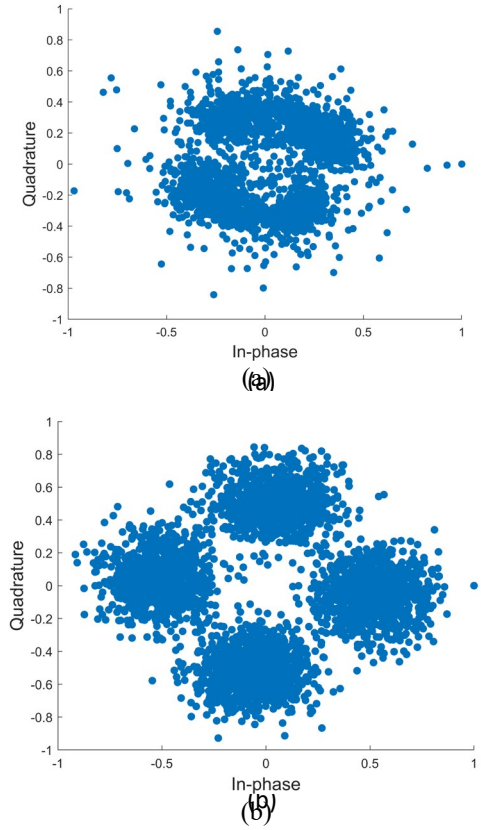

Fig. 12: Snapshot of TFCE-UW-OFDM signals (a) transmitted signal and (b) received signal.

Fig. 13: Constellation plot of the received signal after equalization (a) OFDM and (b) TFCE-UW-OFDM.

the improvement of the proposed approaches vanishes, and such a DS effect estimator must be used in that case. Further, Figs. 10 and 11, illustrate the BER and NMSE performance at different SNR and DS effects values. As shown, the TD-UW-OFDM becomes increasingly sensitive to the Doppler effect in both NMSE and BER performance. Fortunately, that can be tracked and fixed when using TFCE-UW-OFDM at the expense of 3.1% of subcarrier utilization only. That also validates the significant advantage of the proposed approaches in the IoUT-based UWAC environment.

B. Experimental Results

We conducted real tests in the sea of Zhoushan, China, to validate the advantages of the proposed approaches in the UWAC environment. The same parameters from Table 1 were used, except for the DS and multipath effects experienced by the real channel. In the field test, the transmitter was positioned at the port, while the receiver was located on a ship approximately 300 meters away. The depth of both the transmitter and the receiver was set to 4 meters below the water surface. Unlike the simulation tests, the synchronization was estimated using linear LFM segments placed at the beginning and end of each frame, each frame containing 10 symbols. The same synchronization procedure explained earlier was applied. A vector of zeros was inserted between the LFM segments and the transmitted data to avoid interference. Additionally, convolutional encoding with a rate of 1/2 was employed at the transmitter side and Viterbi decoding was used at the receiver for data recovery. Each data transmission was repeated five times. In order to demonstrate the effect of UWAC harsh channel and noise, an example of a snapshot for the transmitted and received packet of TFCE-UW-OFDM is shown in Fig. 12(a) and (b), respectively. The same down-conversion and decoding procedures outlined in Sections II and III were followed to process the received signal. Fig. 13 illustrates the status of the decoded data using a constellation plot. As shown in Fig. 13, the status of the received signal in the case of TFCE-UW-OFDM is better than the conventional OFDM. That is justified by the robustness of the TFCE-UW-OFDM to the residual channel errors. To highlight the impact of the real UWAC channel, Fig. 14 shows the estimated CIRs for frame 1 when

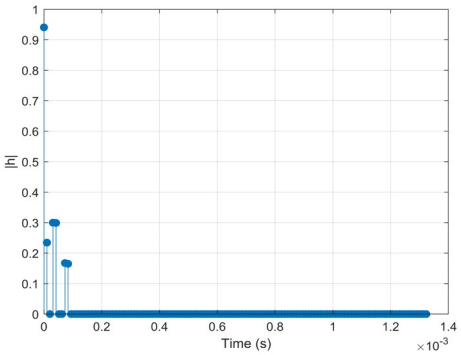

(a)

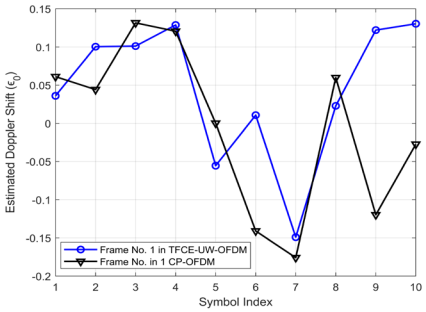

(b)

Fig. 14: UWAC channel effects (a) channel impulse response (Magnitude), and (b) the estimated Doppler effect.

using TFCE-UW-OFDM. In this case, channel coefficients with $|h| < 0.15$ were removed, and the corresponding Doppler effect was observed by tracking the normalized CFO (ϵ_0) for both conventional OFDM and the proposed TFCE-UW-OFDM with the techniques of null subcarriers. It is evident that the real UWAC channel exhibits doubly selective fading, and the proposed scheme demonstrates greater robustness against these impairments. Furthermore, Table 3 presents the BER performance for each transmitted frame. The proposed TD-UW-OFDM and TFCE-OFDM methods outperform conventional OFDM systems in both simulation and real-world scenarios, improving both BER and spectral efficiency (as summarized in Table 2). As a result, these methods represent promising solutions for enhancing the spectral efficiency and reliability of IoUT-based UWAC.

VI. Conclusion

In this paper, we have presented two methods, TD-UW-OFDM and TFCE-UW-OFDM, to improve the reliability of IoUT communication systems against problems caused by underwater acoustic channels. The proposed schemes effectively minimize the overhead required to monitor UWAC channel variations by employing a time-domain guard interval. TD-UW-OFDM works especially well in environments with short-delay UWAC channels because it can track channel effects in an IBI-free area at the end of the time-domain guard interval. The proposed TFCE-UW-OFDM, on the other hand, makes the system more reliable by improving performance in scenarios where an IBI-free region cannot be guaranteed. Both approaches significantly improve bandwidth efficiency by reducing the reliance on extensive pilot data traditionally used for channel tracking. Notably, TFCE-UW-OFDM only needs 3.1% of the frequency-domain subcarriers for this purpose, while traditional UWAC-OFDM systems need 25%. This demonstrates the practicality of our methods in real-world UWAC applications. The results from both simulations and real-world experiments demonstrate that these approaches substantially enhance the performance of IoUT-based UWAC systems, making them strong candidates for the next generation of underwater communication technologies.

References

[1] X. Ma, B. Wang, W. Tian, X. Ding, and Z. Han, "Strategic Game Model for AUV-Assisted Underwater Acoustic Covert Communication in Ocean Internet of Things," *IEEE Internet of Things Journal,* vol. 11, no. 12, pp. 22508 - 22520, 2024.

[2] J. Xu, M. A. Kishk, Q. Zhang, and M.-S. Alouini, "Three-hop underwater wireless communications: A novel relay deployment technique," *IEEE Internet of Things Journal,* vol. 10, no. 15, pp. 13354-13369, 2023.

[3] L. Wan, J. Zhu, E. Cheng, and Z. Xu, "Joint CFO, gridless channel estimation and data detection for underwater acoustic OFDM systems," *IEEE Journal of Oceanic Engineering,* vol. 47, no. 4, pp. 1215-1230, 2022.

[4] H. Wang, W. Jiang, Q. Hu, Z. Zeng, and Z. Li, "Time-varying Channel and Intrablock Carrier Frequency Offset Estimation for OFDM Underwater Acoustic Communication," *IEEE Sensors Journal,* vol. 24, no. 11, pp. 18405 - 18417, 2024.

[5] Z. A. Qasem *et al.*, "Real Signal DHT-OFDM with Index Modulation for Underwater Acoustic Communication," *IEEE Journal of Oceanic Engineering,* vol. 48, no. 1, pp. 246-259, 2023.

[6] Z. A. Qasem, H. A. Leftah, H. Sun, J. Qi, and H. Esmaiel, "X-Transform Time-Domain Synchronous IM-OFDM-SS for Underwater Acoustic Communication," *IEEE Systems Journal,* vol. 16, pp. 1984-1995, 2021.

[7] A. Amar, G. Avrashi, and M. Stojanovic, "Low complexity residual Doppler shift estimation for underwater acoustic multicarrier communication," *IEEE Transactions on Signal Processing,* vol. 65, no. 8, pp. 2063-2076, 2016.

[8] B. Li, S. Zhou, M. Stojanovic, and L. Freitag, "Pilot-tone based ZP-OFDM demodulation for an underwater acoustic channel," presented at the in Proc. MTS/IEEE OCEANS Conf, Boston , MA, Sep. 18–21, 2006, CD-ROM.

[9] B. Li, S. Zhou, M. Stojanovic, L. Freitag, and P. Willett, "Non-uniform Doppler compensation for zero-padded OFDM over fast-varying underwater acoustic channels," presented at the in Proc. MTS/IEEE OCEANS Conf., , Aberdeen, Scotland, Jun., 2007.

[10] J. Huang and R. Diamant, "Adaptive modulation for long-range underwater acoustic communication," *IEEE Transactions on Wireless Communications,* vol. 19, no. 10, pp. 6844-6857, 2020.

[11] K. Tu, T. M. Duman, M. Stojanovic, and J. G. Proakis, "Multiple-resampling receiver design for OFDM over Doppler-distorted underwater acoustic channels," *IEEE Journal of Oceanic Engineering,* vol. 38, no. 2, pp. 333-346, 2012.

[12] B. Li, S. Zhou, M. Stojanovic, L. Freitag, and P. Willett, "Multicarrier communication over underwater acoustic channels with nonuniform Doppler shifts," *IEEE Journal of Oceanic Engineering,* vol. 33, no. 2, pp. 198-209, 2008.

[13] T. Kang and R. A. Iltis, "Iterative carrier frequency offset and channel estimation for underwater acoustic OFDM systems," *IEEE Journal on Selected Areas in Communications,* vol. 26, no. 9, pp. 1650-1661, 2008.

[14] J. Tao, "DFT-precoded MIMO OFDM underwater acoustic communications," *IEEE Journal of Oceanic Engineering,* vol. 43, no. 3, pp. 805-819, 2017.

[15] H. Esmaiel and D. Jiang, "Zero-pseudorandom noise training OFDM," *Electronics Letters,* vol. 50, no. 9, pp. 650-652, 2014.

[16] N. U. R. Junejo, H. Esmaiel, M. Zhou, H. Sun, J. Qi, and J. Wang, "Sparse Channel Estimation of Underwater TDS-OFDM System using Look-ahead Backtracking Orthogonal Matching Pursuit," *IEEE Access,* vol. 6, pp. 74389-74399, 2018.

[17] B. Wang, Y. Ge, C. He, Y. Wu, and Z. Zhu, "Study on communication channel estimation by improved SOMP based on

distributed compressed sensing," *EURASIP Journal on Wireless Communications and Networking,* vol. 2019, no. 121 pp. 1-8, 2019.

[18] W. Dai and O. Milenkovic, "Subspace pursuit for compressive sensing signal reconstruction," *IEEE transactions on Information Theory,* vol. 55, no. 5, pp. 2230-2249, 2009.

[19] D. Sundman, S. Chatterjee, and M. Skoglund, "A greedy pursuit algorithm for distributed compressed sensing," in *2012 IEEE International Conference on Acoustics, Speech and Signal Processing (ICASSP)*, 2012: IEEE, pp. 2729-2732.

[20] X. Jiang, W.-J. Zeng, E. Cheng, and C.-R. Lin, "Multipath channel estimation using fast least-squares algorithm," in *2011 Third International Conference on Communications and Mobile Computing*, 2011: IEEE, pp. 433-436.

[21] D. Ren, J. Li, G. Lu, and J. Ge, "Per-subcarrier RLS adaptive channel estimation combined with channel equalization for FBMC/OQAM systems," *IEEE Wireless Communications Letters,* vol. 9, no. 7, pp. 1036-1040, 2020.

[22] A. Soysal, S. Ulukus, and C. Clancy, "Channel estimation and adaptive M-QAM in cognitive radio links," in *2008 IEEE International Conference on Communications*, 2008: IEEE, pp. 4043-4047.

[23] L. Dai, Z. Wang, and Z. Yang, "Time-frequency training OFDM with high spectral efficiency and reliable performance in high speed environments," *IEEE Journal on Selected Areas in Communications,* vol. 30, no. 4, pp. 695-707, 2012.

[24] L. Dai, Z. Wang, and Z. Yang, "Spectrally efficient time-frequency training OFDM for mobile large-scale MIMO systems," *IEEE Journal on Selected Areas in Communications,* vol. 31, no. 2, pp. 251-263, 2013.

[25] C. Hofbauer, W. Haselmayr, H.-P. Bernhard, and M. Huemer, "On the inclusion and utilization of pilot tones in unique word OFDM," *IEEE Transactions on Signal Processing,* vol. 68, pp. 5504-5518, 2020.

[26] H. Steendam, "Theoretical performance evaluation and optimization of UW-OFDM," *IEEE Transactions on Communications,* vol. 64, no. 4, pp. 1739-1750, 2016.

[27] M. Rajabzadeh and H. Steendam, "Precoding for PAPR reduction in UW-OFDM," *IEEE Communications Letters,* vol. 25, no. 7, pp. 2305-2308, 2021.

[28] Z. A. Qasem, J. Wang, X. Kuai, H. Sun, and H. Esmaiel, "Enabling Unique Word OFDM for Underwater Acoustic Communication," *IEEE Wireless Communications Letters,* vol. 10, no. 9, pp. 1886 - 1889, 2021.

[29] M. Rajabzadeh and H. Steendam, "Power spectral analysis of UW-OFDM systems," *IEEE Transactions on Communications,* vol. 66, no. 6, pp. 2685-2695, 2017.

[30] M. Rajabzadeh, H. Khoshbin, and H. Steendam, "Sidelobe suppression for non-systematic coded UW-OFDM in cognitive radio networks," in *European Wireless 2014; 20th European Wireless Conference*, 2014: VDE, pp. 1-6.

[31] F. Haddad, C. Bockelmann, and A. Dekorsy, "Channel Estimation and Pilot Overhead Reduction in OFDM Systems using Compressed Sensing Dynamic Mode Decomposition," *IEEE Communications Letters,* vol. 28, no. 5, pp. 1137 - 1140, 2024.

[32] J. Du, Y. Chen, P. Zhang, S. Mumtaz, X. Li, and D. B. Da Costa, "An Effective Simultaneous Channel Estimation and Sensing Algorithm for MmWave MIMO-OFDM Systems," *IEEE Transactions on Wireless Communications,* vol. 23, no. 11, pp. 17054 - 17069, 2024.

[33] W.-G. Song and J.-T. Lim, "Channel estimation and signal detection for MIMO-OFDM with time varying channels," *IEEE Communications Letters,* vol. 10, no. 7, pp. 540-542, 2006.

[34] I. Singh, S. Kalyani, and K. Giridhar, "A practical compressed sensing approach for channel estimation in OFDM systems," *IEEE Communications Letters,* vol. 19, no. 12, pp. 2146-2149, 2015.

[35] Z. Tang, R. C. Cannizzaro, G. Leus, and P. Banelli, "Pilot-assisted time-varying channel estimation for OFDM systems," *IEEE Transactions on Signal Processing,* vol. 55, no. 5, pp. 2226-2238, 2007.

[36] S. M. Kay, "Fundamentals of Statistical Signal Processing: Estimation Theory," ed: Prentice Hall, 1993.

[37] A. Ijaz, A. Awoseyila, and B. Evans, "Low-complexity time-domain SNR estimation for OFDM systems," *Electronics letters,* vol. 47, no. 20, pp. 1154-1156, 2011.

[38] B. Li, S. Zhou, and M. Stojanovic, "Multicarrier Communication Over Underwater Acoustic Channels With Nonuniform Doppler Shifts," *IEEE Journal of Oceanic Engineering,* vol. 33, no. 2, pp. 198-209, 2008.

[39] P. Qarabaqi and M. Stojanovic, "Statistical characterization and computationally efficient modeling of a class of underwater acoustic communication channels," *IEEE Journal of Oceanic Engineering,* vol. 38, no. 4, pp. 701-717, 2013.

[40] H. A. Leftah and S. Boussakta, "Novel OFDM based on C-transform for improving multipath transmission," *IEEE Transactions on Signal Processing,* vol. 62, no. 23, pp. 6158-6170, 2014.